Catalysis Communications 18 (2012) 93–97

Contents lists available at SciVerse ScienceDirect

Catalysis Communications

journal homepage: www.elsevier.com/locate/catcom

Short Communication

Preparation of PbYO composite photocatalysts for degradation of methyl orange under visible-light irradiation

Tong-ming Su [a], Zi-li Liu [a,b], Yi Liang [a], Zu-zeng Qin [a,*], Jie Liu [a], Yan-qiu Huang [a]

[a] *School of Chemistry and Chemical Engineering, Guangxi University, Nanning 530004, Guangxi, China*
[b] *School of Chemistry and Chemical Engineering, Guangzhou University, Guangzhou 510006, Guangdong, China*

ARTICLE INFO

Article history:
Received 23 September 2011
Received in revised form 18 November 2011
Accepted 21 November 2011
Available online 28 November 2011

Keywords:
Lead yttrium oxide
Visible-light irradiation
Photocatalytic degradation
Methyl orange

ABSTRACT

The PbYO composites were prepared through a precipitation method and used for the degradation of methyl orange under visible-light irradiation. The PbYO complex photocatalysts were characterized by X-ray diffraction (XRD), UV–vis diffuse reflectance spectroscopy, N_2 adsorption–desorption, and terephthalic acid photoluminescence (TA-PL) probing technique. The results indicated that the photodegradation of methyl orange was significantly enhanced in the presence of PbYO complex oxide when compared with $BiYO_3$. The calcination temperature was found to have a significant effect on the photocatalytic activity of PbYO composites. Specifically, PbYO calcined at 800 °C had a considerably larger surface area, lower reflectance intensity, higher formation rate of free ·OH radicals and showed higher photocatalytic activity.

1. Introduction

In recent years, azo dyes have become the largest group of colorants used in a variety of industries, such as textiles, foodstuffs, leather and color printing. As a result, more and more azo dyes appear in industrial wastewater [1,2]. Without effective treatment, releases of this wastewater can result in environmental pollution that is manifested in water coloration and toxicity [3]. On the other hand, solar spectrum photocatalysis is attracting more attention as a possible means of environmental remediation and the generation of clean H_2 from water, and photocatalysis also plays an important role in today's wastewater treatment technologies. Research has been conducted to shift the optical absorption edge of TiO_2 to lower energies and increase the photocatalytic activity in the visible-light range. Studies have shown that doping TiO_2 with nonmetal or metal atoms, such as N [4], S [5], I [6], Sn [7] and Au [8] have increased the catalytic activity in visible light. At the same time, many other novel materials, such as SnO_x-$ZnGa_2O_4$ [9], Ag/AgCl/BiOCl [10], $ZnCo_2O_4$ [11] and BiOI/BiOBr [12] have attracted great interest because of their properties and potential for utilizing solar energy in photocatalysis.

Yttrium is a kind of rare earth metal with an outer shell electron distribution of $4d^15s^2$, (i. e., that is, only one d electron exists which can receive pair with other electrons and to form a half-full or full-filled type while maintaining with a stable electron distribution on the yttrium d orbital). In terms of photocatalytic activity, some Y complexes involve complex oxides, such as $TiO_2/YFeO_3$ [13], Er^{3+}: $YAlO_3/TiO_2$ [14], $BiYO_3$ [15], and $InYO_3$ [16]. On the other hand, there are several studies about the applications of $PbWO_4$ as photocatalysts, $PbWO_4$ has also received considerable attention as an agent for degrading organic dyes photolytically [17–20].

The present work builds on the previous work with $BiYO_3$ [15], $InYO_3$ [16], $PbWO_4$ [20], and $Bi_xY_{(2-x)}O_3$ [21] and reports on the synthesis and selected properties of PbYO composite oxide photocatalysts as revealed by thermo analysis, X-ray diffraction (XRD), UV–visible diffuse reflectance spectroscopy, N_2 adsorption, and the degradation of methyl orange(MO) under visible-light irradiation.

2. Experimental

2.1. Preparation and characterization of PbYO photocatalysts

The PbYO composite oxide photocatalysts were prepared by chemical precipitation method. $Pb(NO_3)_2$ and $Y(NO_3)_3$ were weighted by 1:1 in molar ratio and prepared 0.1 mol L^{-1} solution, respectively. $Pb(NO_3)_2$ solution was added drop-wise to an equal volume of $Y(NO_3)_3$ solution. The mixture was adjusted to pH = 8 by adding 0.5 mol L^{-1} NH_4OH solution while stirring to yield a white precipitate. The precipitate was filtered and washed with distilled water and dried for 10 h at 90 °C, resulting in the PbYO precursor. The precursor was ground to pass through a 100-mesh sieve mesh. Different samples of photocatalysts were obtained by calcining the precursor for 2 h at 500, 600, 700, 800, and 900 °C, respectively. As a comparison, a sample of $BiYO_3$ was prepared and tested as described in previous work [15].

X-ray diffraction analysis was performed using an XD-3 X-ray powder diffraction instrument (Beijing Purkinje General Instrument

---

* Corresponding author. Tel.: +86 771 3272702; fax: +86 771 3233718.
E-mail address: qinzuzeng@gmail.com (Z. Qin).

1566-7367/$ – see front matter © 2011 Elsevier B.V. All rights reserved.
doi:10.1016/j.catcom.2011.11.027

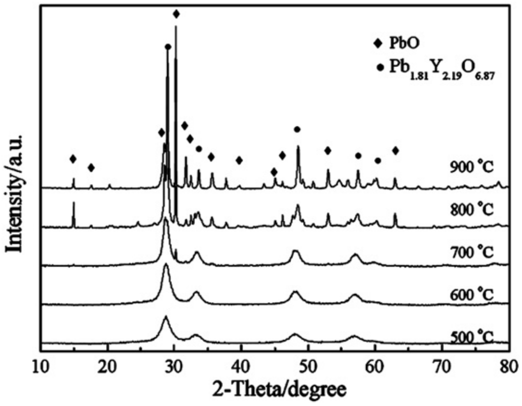

Fig. 1. XRD patterns of PbYO composite photocatalysts calcined at different temperatures.

Co., Ltd), equipped with a Cu *Kα* radiation source. UV–vis diffuse reflectance spectra were obtained using a UV–vis spectrometer (Shimadzu. UV-2501 PC). N_2 adsorption–desorption was conducted in a ASAP 2020 Physisorption analyzer (Micromeritics Instrument Corporation), based on the adsorption branches of N_2 sorption isotherms, the Brunauer–Emmett–Teller (BET) method was used to calculate the specific surface area and the Barrett–Joyner–Halenda (BJH) model was used to calculate the pore volume and average pore radius of the catalyst under study.

Photoluminescence (PL) technique with terephthalic acid as a probe molecule was used to detect the formation of free·OH radicals on the surface of the UV-illuminated photocatalyst. The experiment produced at ambient temperature, 0.1 g of the PbYO composite photocatalyst calcined at different temperatures or $BiYO_3$ was dispersed in 20 mL of the 5×10^{-4} mol L^{-1} terephthalic acid aqueous solution with a concentration of 2×10^{-3} mol L^{-1} NaOH in a dish with a diameter of about 9.0 cm. A 15 W, 365 nm UV lamp (6 cm above the dishes) was used as a light source. After UV irradiated for 30 min, the reaction solution was centrifuged and filtrated to measure the increasing amount in the PL intensity on a fluorescence spectrophotometer (Shimadzu RF-5301PC) at 425 nm excited by 315 nm light of 2-hydroxyterephthalic acid.

2.2. Photocatalytic degradation of MO

The investigation of the photocatalytic degradation of MO was conducted as previously described in the literature [15].

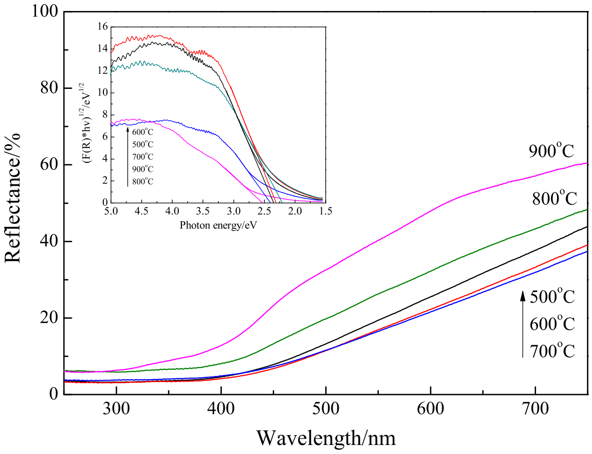

Fig. 2. UV–visible diffuse reflectance spectra of PbYO composite photocatalysts calcined at different temperatures.

Table 1
The absorption edge and band energy (E_g) of PbYO composite photocatalysts calcined at different temperature.

Calcination temperature (°C)	Absorption edge (nm)	E_g (eV)
500	530	2.34
600	534	2.32
700	559	2.22
800	508	2.44
900	484	2.56

3. Results and discussion

3.1. Results of photocatalyst characterization

Calcination temperature is an important factor that can affect the structure of the catalyst. X-ray diffraction (XRD) was used to identify the crystalline phases of the calcined PbYO samples. XRD patterns of the samples calcined at 500 °C, 600 °C, 700 °C, 800 °C, and 900 °C are shown in Fig. 1.

From Fig. 1, it can be seen that $Pb_{1.81}Y_{2.19}O_{6.78}$ (JCPDS: 47-0873) was produced in crystalline form after being calcined at 500 °C or 600 °C for 2 h, and obvious diffraction peaks of $Pb_{1.81}Y_{2.18}O_{6.78}$ were found at $2\theta = 29.1^{\circ}$, 33.7°, 48.4°, 57.4°. In addition, very weak PbO (JCPDS: 65-2809) diffraction peaks were found at $2\theta = 15.0^{\circ}$, 29.1° and 30.3° in the sample calcined at 700 °C. In the samples calcined at 800 °C, additional diffraction peaks of PbO (JCPDS: 65-2809) were found at $2\theta = 17.7^{\circ}$, 28.6°, 31.8°, 35.8°, and 48.6°, with the dominant growth surface of the crystal being the plane (112) at $2\theta = 30.3^{\circ}$. The intensity of the diffraction peaks of PbO in the sample calcined at 900 °C was obviously decreased, which indicates that the content of PbO in the sample had decreased at this higher temperature.

The UV–vis diffuse reflectance spectra of the PbYO composite photocatalysts calcined at different temperatures for 2 h are shown in Fig. 2. The samples exhibit absorption extending from the UV to the infrared, with the most significant differences appearing in the spectra of samples calcined at the two highest temperatures. When calcined at 500 °C and 600 °C, the absorption edge was at 530 nm and 534 nm, respectively. When calcined above 700 °C, the reflectance of visible light from the PbYO complexes increased with the increasing of calcination temperatures. At the highest temperature the maximum reflectance was only about 70%, while the absorption edge was blue shifted for 559 nm to 453 nm with the increasing of calcination temperatures. In summary, these spectra show that visible light is well absorbed by the PbYO photocatalysts.

For a semiconductor sample, it is possible to determine the optical absorption near the band edge from the Kubelka–Munk method: $\alpha h\nu = A(h\nu - E_g)^{n/2}$ [22], where α, h, ν, E_g and A are absorption coefficient, Planck constant, radiation frequency, band gap and a constant, respectively. From the inset in Fig. 2, the absorption edges of PbYO calcined at different temperatures were found and the band gap can be calculated from the above equation, and the data were shown in Table 1.

As shown in Table 1, the band gap of the PbYO samples calcined at 500 °C, 600 °C and 700 °C decreased, while the absorption edges moved to longer wavelengths, which indicated the increasing of visible-light absorption. As the calcination temperature increased from 700 to 900 °C, the band gap increased from 2.22 eV to 2.56 eV. Combining these results with the results of the XRD above, it appears that in samples calcined at higher temperatures, a PbO and $Pb_{1.81}Y_{2.19}O_{6.78}$ mixture was generated from the PbYO precursor, which caused a deterioration of its absorption performance of visible light.

Fig. 3 shows the N_2 adsorption–desorption isotherm and the pore size distribution of PbYO samples calcined at different temperatures.

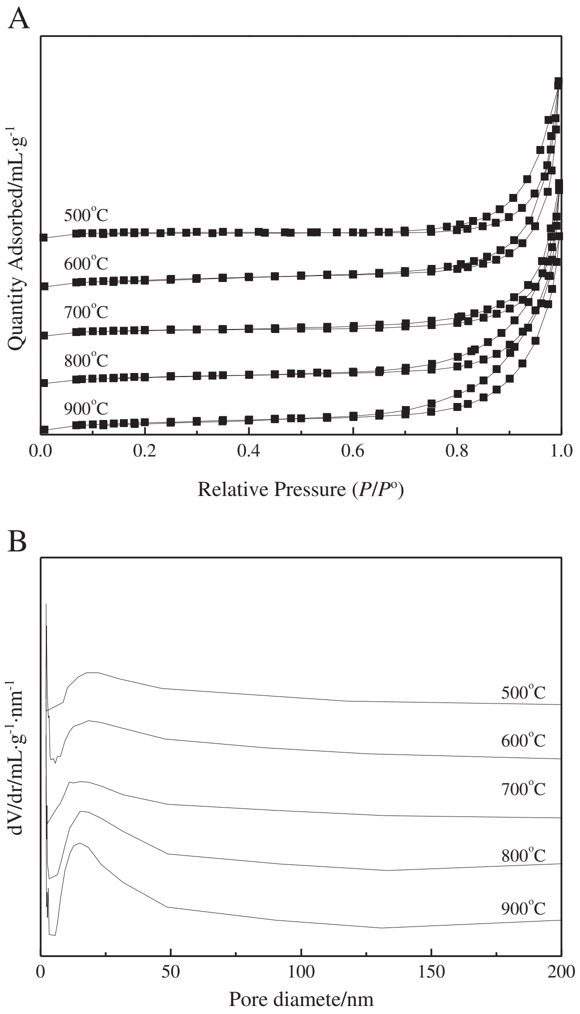

Fig. 3. N_2 adsorption–desorption isotherm (A) and pore size distribution curve (B) of PbYO composite photocatalysts calcined at different temperatures.

As shown in Fig. 3A, the N_2 isotherm adsorption of PbYO composite photocatalysts calcined at different temperatures belonged to the III-type isotherm with a hysteresis loop. The isotherm plot of PbYO composite photocatalysts calcined at different temperatures both has a region of mildly increasing N_2 adsorption at low relative pressure ($P/P_0 < 0.5$) which can be related to the transfer from the monolayer adsorption to the multilayer N_2 adsorption on the PbYO composite photocatalysts surface [23,24]. Regarding desorption, the PbYO composite photocatalysts prepared at different temperatures had H3-type hysteresis loops, and the relative pressure of the desorption branches was $0.50 < P/P_0 < 1.0$. This value indicated that the PbYO composite photocatalysts prepared at the studied temperatures was sheet material with oblique slit-like holes. It can be seen in Fig. 3A that the start and end of the hysteresis loops of PbYO composite photocatalysts calcined at 800 °C were the widest, which indicated that the amount of adsorption and desorption was the largest according to the capillary condensed theory and Kelvin equation [24]. Therefore, the pore size distribution was most narrow for the catalyst calcined at 800 °C.

Table 2
Textural properties of PbYO composite photocatalysts.

Calcination temperature/°C	BET surface area/$m^2\ g^{-1}$	Total pore volume/ 10^{-2} mL g^{-1}	Average pore diameter/nm
500	3.3	2.44	20.2
600	3.5	1.94	17.2
700	3.8	1.75	18.4
800	4.4	2.36	21.6
900	2.6	2.50	19.1

In accordance with the N_2 adsorption isotherm–desorption data of PbYO composite photocatalysts, the surface area, pore volume, and average pore radius from the Brunauer–Emmett–Teller (BET) and Barrett–Joyner–Halenda (BJH) methods are shown in Table 2.

From the pore size distribution data of PbYO composite photocatalysts calcined at different temperatures shown in Fig. 3B and Table 2, it can be seen that the pores in the photocatalysts mainly are mesoporous, with an average pore diameter of 20 nm and very small amounts of microporosity.

From Table 2, it can be seen that the specific surface area of PbYO catalysts was little changed when the calcination temperature ranged from 500 °C to 900 °C, although the maximum surface area of 4.4 $m^2\ g^{-1}$ was observed at the calcination temperature of 800 °C, reducing to 2.6 $m^2\ g^{-1}$ when the calcination temperature was increased to 900 °C. With the increase of the calcination temperature, the average pore diameter was reduced and the catalysts may sinter at high temperature which could result in a decrease of the photocatalytic activity. The pore volumes of the catalysts calcined at different temperatures have small changes. However, the average pore diameter of the catalyst was a maximum at the calcination temperature of 800 °C, which may account for the observation below that photocatalytic activity was highest for the sample calcined at 800 °C.

Hydroxyl radicals are known as an important reaction species in the photocatalytic process [10,25]. Terephthalic acid reacts with ·OH readily to produce a highly fluorescent product, 2-hydroxyterephthalic acid, whose PL peak intensity is in proportion to the amount of OH radicals produced in water [26–30]. The formation of hydroxyl radicals (·OH) on the surface of UV-illuminated PbYO composite photocatalyst is detected by PL with terephthalic acid as a probe molecule. Fig. 4 shows the change of PL spectra of the PbYO composite photocatalyst calcined at different temperatures or $BiYO_3$. From Fig. 4, it can be seen that an obvious difference in PL intensity at about 425 nm is observed in different samples. For the PbYO composite photocatalyst calcined at 800 °C, the formation rate of ·OH radicals on its surface is much higher than that of other samples. The PL intensity of $BiYO_3$, the reference catalyst, is only a little higher than that of PbYO calcined at 500 °C and the pure terephthalic acid. It suggests that the surface of PbYO composite photocatalysts inhibits the production of ·OH radicals when the calcination temperature is lower or higher than 800 °C, which implies that when the calcination temperature is 800 °C, the photocatalytic oxidation activity of the photocatalyst is much higher than any other photocatalysts.

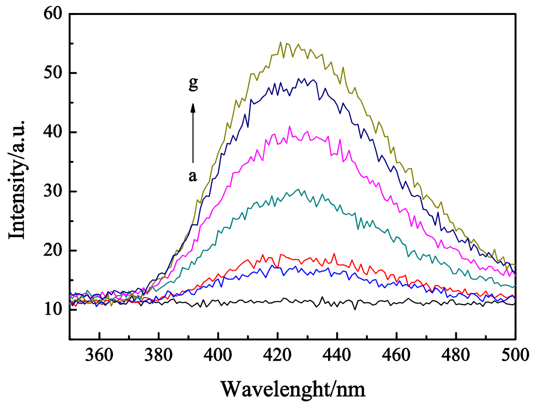

Fig. 4. PL spectral changes of pure terephthalic acid (a), $BiYO_3$ (c) and the PbYO composite photocatalysts calcined at 500 °C (b), 600 °C (d), 700 °C (e), 800 °C (f), 900 °C (g).

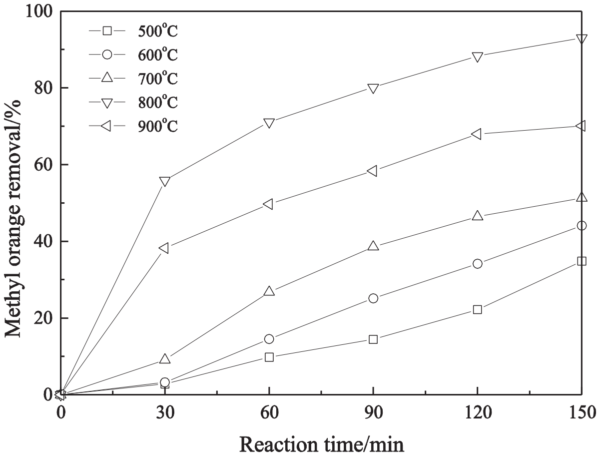

Fig. 5. Effects of calcination temperature on PbYO composite photocatalysts catalytic degradation of methyl orange under visible-light irradiation.

3.2. Photocatalytic degradation of MO under visible-light irradiation

Fig. 5 shows the results of using the samples of PbYO calcined at different temperatures as photocatalysts with visible light. The data show that the calcination temperature has a significant effect on the degradation results.

Specifically, after irradiation by visible light for 150 min, the degradation of methyl orange was 34.8%, 44.1%, 51.3%, 93.0%, and 70.1%, respectively, using the PbYO composite oxides calcined at 500 °C, 600 °C, 700 °C, 800 °C, and 900 °C as photocatalysts. The degradation data of MO show that the optimal calcination temperature of the PbYO composite photocatalyst is 800 °C. As noted above in the discussion of the XRD results, when the calcination temperatures lower than 700 °C, only a single phase of $Pb_{1.81}Y_{2.18}O_{6.78}$ was found in the PbYO catalyst. However, when calcined at 800 °C and 900 °C not only $Pb_{1.81}Y_{2.18}O_{6.78}$ but also PbO was found in the PbYO composite photocatalysts, and a heterostructure may form between the $Pb_{1.81}Y_{2.18}O_{6.78}$ and PbO phases. In general, when a kind of hetero structure material forms between two or more different materials, more lattice defects will be generated which are usually the active sites of a photocatalyst [31]. For a catalytic process, defect states may be formed between the band gaps of the catalysts and the lattice defects [32], which lead to the PbYO complex photocatalyst being excited by visible light and showing higher photocatalytic activity. Therefore, even the catalysts calcined at 500 °C, 600 °C, and 700 °C can absorb more visible light and have a narrower band gap. The PbYO complex photocatalysts calcined at 800 °C and 900 °C formed heterostructures inside the catalysts and show better photocatalytic activity for their larger specific surface areas, larger pore diameters and pore volumes. Combined with the PL intensity of the samples, the formation rate of ·OH radicals in water solution of the PbYO composite photocatalyst calcined at 800 °C is much larger than that of other samples. Oxidized by more high activity free ·OH radicals species with higher oxidizing ability, the MO molecule was destroyed. The degradation data of MO was consistent with the characterization results of the present photocatalyst.

The kinetics of the MO degradation were found to fit a pseudo-first order model by plotting $-\ln(c/c_0)$ versus reaction (t), as shown in Table 3.

The above results show that the reaction rate constant of photocatalytic degradation of methyl orange of PbYO composite photocatalyst calcined at 800 °C was 0.01681 min^{-1}, which was 6.18 times higher than the rate observed with the PbYO composite photocatalyst calcined at 500 °C, and the data indicated that there are great effects of calcination temperature on the photocatalytic activities of PbYO complex oxides. At the same time, compared with $BiYO_3$ [15], the reaction rate constant of PbYO photocatalyst calcined at 800 °C is 8.6 times than that of $BiYO_3$ photocatalyst calcined at 750 °C.

Table 3
Degradation rate as a function of calcination temperatures and pseudo-first order rate constants derived from fitting experimental data to computer model.

Calcination temperature (°C)	Rate constant (10^{-3} min^{-1})	Correlation coefficient, R^2
500	2.72	0.9621
600	3.99	0.9874
700	5.10	0.9930
800	16.81	0.9934
900	7.81	0.9736

4. Conclusions

The preparation of PbYO complex photocatalysts calcined at different temperatures were characterized and evaluated for their photocatalytic activity in degrading methyl orange under visible-light irradiation. It was found that these photocatalysts have good visible-light absorption. The calcination temperature was found to have a significant effect on photocatalytic activity of the materials. The complex photocatalyst calcined at 800 °C appeared to have a heterojunction structure of PbO and $Pb_{1.81}Y_{2.18}O_{6.78}$ with a band gap of 2.44 eV and exhibited the highest photoactivity.

Acknowledgements

This work was supported by the National Natural Science Foundation of China (21006013), the Scientific Research Foundation of Guangxi University (XBZ090780) and the National Students Innovation Experiment Program in Guangxi University (201017). We also thank Dr. Donald G. Barnes for his helpful discussions about language of the paper.

References

[1] M. Saquib, M. Muneer, Titanium dioxide mediated photocatalyzed degradation of a textile dye derivative, acid orange 8, in aqueous suspensions, Desalination 155 (2003) 255–263.
[2] A. Rehorek, M. Tauber, G. Gübitz, Application of power ultrasound for azo dye degradation, Ultrasonics Sonochemistry 11 (2004) 177–182.
[3] J. Hong, H. Emori, M. Otaki, Photodecolorization of azo dyes by extracellular metabolites under fluorescent light and influence of operational parameters, Journal of Bioscience and Bioengineering 100 (2005) 192–196.
[4] Y. Xin, H. Liu, L. Han, Study on mechanism of enhanced photocatalytic performance of N-doped TiO_2/Ti photoelectrodes by theoretical and experimental methods, Journal of Materials Science 46 (2011) 7822–7829.
[5] C. Han, M. Pelaez, V. Likodimos, A.G. Kontos, P. Falaras, K. O'Shea, D.D. Dionysiou, Innovative visible light-activated sulfur doped TiO_2 films for water treatment, Applied Catalysis B: Environmental 107 (2011) 77–87.
[6] Q. Zhang, Y. Li, E.A. Ackerman, M. Gajdardziska-Josifovska, H. Li, Visible light responsive iodine-doped TiO_2 for photocatalytic reduction of CO_2 to fuels, Applied Catalysis A 400 (2011) 195–202.
[7] V.B.R. Boppana, R.F. Lobo, Photocatalytic degradation of organic molecules on mesoporous visible-light-active Sn(II)-doped titania, Journal of Catalysis 281 (2011) 156–168.
[8] B. Cojocaru, Ş. Neaţu, E. Sacaliuc-Pârvulescu, F. Lévy, V.I. Pârvulescu, H. Garcia, Influence of gold particle size on the photocatalytic activity for acetone oxidation of Au/TiO_2 catalysts prepared by dc-magnetron sputtering, Applied Catalysis B: Environmental 107 (2011) 140–149.
[9] V.B.R. Boppana, R.F. Lobo, SnO_x–$ZnGa_2O_4$ photocatalysts with enhanced visible light activity, ACS Catalysis 1 (2011) 923–928.
[10] W. Xiong, Q. Zhao, X. Li, D. Zhang, One-step synthesis of flower-like Ag/AgCl/BiOCl composite with enhanced visible-light photocatalytic activity, Catalysis Communications 16 (2011) 229–233.
[11] B. Cui, H. Lin, X.C. Zhao, J.B. Li, W.D. Li, Visible light induced photocatalytic activity of $ZnCo_2O_4$ nanoparticles, Acta Physico-Chimica Sinica 27 (2011) 2411–2415.
[12] J. Cao, B. Xu, B. Luo, H. Lin, S. Chen, Novel BiOI/BiOBr heterojunction photocatalysts with enhanced visible light photocatalytic properties, Catalysis Communications 13 (2011) 63–68.
[13] W. Wang, S. Li, Y. Wen, M. Gong, L. Zhang, Y. Yao, Y. Chen, Synthesis and characterization of TiO_2/$YFeO_3$ and its photocatalytic oxidation of gaseous benzene, Acta Physico-Chimica Sinica 24 (2008) 1761–1766.

[14] J. Wang, Y. Xie, Z. Zhang, J. Li, C. Li, L. Zhang, Z. Xing, R. Xu, X. Zhang, Photocatalytic degradation of organic dyes by Er^{3+}:$YAlO_3$/TiO_2 composite under solar light, Environmental Chemistry Letters 8 (2010) 87–93.

[15] Z.-z. Qin, Z.-l. Liu, Y.-b. Liu, K.-d. Yang, Synthesis of $BiYO_3$ for degradation of organic compounds under visible light irradiation, Catalysis Communications 10 (2009) 1604–1608.

[16] Z.-z. Qin, Y. Liang, Z.-l. Liu, W.-q. Jiang, Preparation of $InYO_3$ catalyst and its application in photodegradation of molasses fermentation wastewater, Journal of Environmental Sciences 23 (2011) 1219–1224.

[17] J.-m. Lin, J.-m. Xie, X.-m Lv, Sh.-p. Hu, M. Zhang, Synthesis of nanocrystalline $PbWO_4$ photocatalyst assisted with ultrasonic, Journal of the Chinese Ceramic Society 35 (2007) 1503–1507.

[18] M.W. Stoltzfus, P.M. Woodward, R. Seshadri, J.H. Klepeis, B. Bursten, Structure and bonding in $SnWO_4$, $PbWO_4$, and $BiVO_4$: lone pairs vs inert pairs, Inorganic Chemistry 46 (2007) 3839–3850.

[19] O.M. Bordun, A.T. Stets'kiv, Fundamental absorption edge of thin $PbWO_4$ films, Journal of Applied Spectroscopy 67 (2000) 888–892.

[20] Z.-z. Qin, Z.-l. Liu, K.-d. Yang, J.-h. Wei, Degradation of molasses fermentation wastewater by $PbWO_4$ photocatalyst, Journal of Chemical Engineering of Chinese Universities 23 (2009) 339–344.

[21] M.-g. Fan, Z.-z. Qin, Z.-l. Liu, T.-m. Su, Preparation of $Bi_xY_{(2-x)}O_3$ and photocatalytic degradation of molasses fermentation wastewater on it under visible-light irradiation, Advances in Materials Research 287–290 (2011) 1640–1645.

[22] M.A. Butler, Photoelectrolysis and physical properties of the semiconducting electrode WO_3, Journal of Applied Physics 48 (1977) 1914–1920.

[23] F. Rouquerol, J. Rouquerol, K. Sing, Adsorption by powders and porous solids, principles, methodology and applications, Academic Press, San Diego, 1999.

[24] H. Qi, J. Ma, P.-z. Wong, Adsorption isotherms of fractal surfaces, Colloids and Surfaces A: Physicochemical and Engineering Aspects 206 (2002) 401–407.

[25] B. Detlef, Photocatalytic water treatment: solar energy applications, Solar Energy 77 (2004) 445–459, doi: 10.1016/j.solener.2004.03.031.

[26] W. Liu, M. Ji, S. Chen, Preparation, characterization and activity evaluation of $Ag_2Mo_4O_{13}$ photocatalyst, Journal of Hazardous Materials 186 (2011) 2001–2008.

[27] J. Yu, W. Wang, B. Cheng, B.-L. Su, Enhancement of photocatalytic activity of mesoporous TiO_2 powders by hydrothermal surface fluorination treatment, Journal of Physical Chemistry C 113 (2009) 6743–6750.

[28] M. Anpo, M. Che, Applications of photoluminescence techniques to the characterization of solid surfaces in relation to adsorption, catalysis, and photocatalysis, in: B.C.G. Werner, O. Haag, K. Helmut (Eds.), Advances in Catalysis, Academic Press, 1999, pp. 119–257.

[29] Q. Xiao, Z. Si, J. Zhang, C. Xiao, X. Tan, Photoinduced hydroxyl radical and photocatalytic activity of samarium-doped TiO_2 nanocrystalline, Journal of Hazardous Materials 150 (2008) 62–67.

[30] K.-i. Ishibashi, A. Fujishima, T. Watanabe, K. Hashimoto, Detection of active oxidative species in TiO_2 photocatalysis using the fluorescence technique, Electrochemistry Communications 2 (2000) 207–210.

[31] Z. Li, T. Yu, Z. Zou, J. Ye, Degradation in photocatalytic activity induced by hydrogen-related defects in nano-$LiNbO_3$ material, Applied Physics Letters 88 (2006) 071917.

[32] C. Liu, Y.-c. Tu, Y.-s. Luo, Preparation and photocatalytic property of the defect-abundant carbon nanotubes (Natural Science), Journal of Henan Normal University 36 (2008) 70–73.